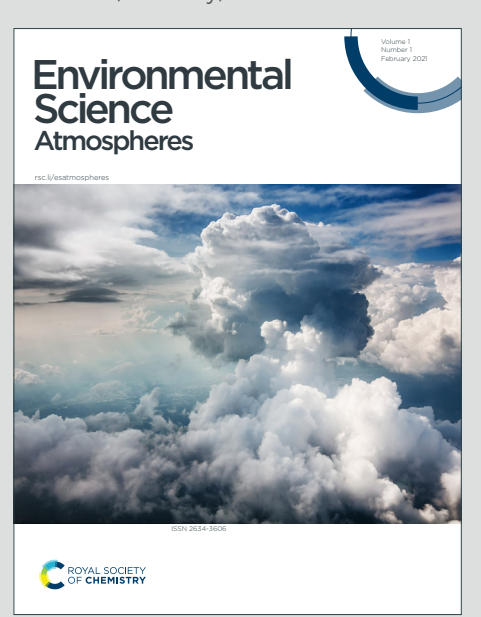


Environmental Science Atmospheres



Accepted Manuscript

This article can be cited before page numbers have been issued, to do this please use: K. Nguyen, M. Schervish, P. Lakey, J. N. Smith and M. Shiraiwa, *Environ. Sci.: Atmos.*, 2025, DOI: 10.1039/D5EA00069F.



This is an Accepted Manuscript, which has been through the Royal Society of Chemistry peer review process and has been accepted for publication.

Accepted Manuscripts are published online shortly after acceptance, before technical editing, formatting and proof reading. Using this free service, authors can make their results available to the community, in citable form, before we publish the edited article. We will replace this Accepted Manuscript with the edited and formatted Advance Article as soon as it is available.

You can find more information about Accepted Manuscripts in the <u>Information for Authors</u>.

Please note that technical editing may introduce minor changes to the text and/or graphics, which may alter content. The journal's standard <u>Terms & Conditions</u> and the <u>Ethical guidelines</u> still apply. In no event shall the Royal Society of Chemistry be held responsible for any errors or omissions in this Accepted Manuscript or any consequences arising from the use of any information it contains.



2

3

4

5

6

8

9

10

11

12

13

14

15

16

17

18

19

20

21

22

23

24

25

26

27

28

29

30

Impact of Particle Phase State on the Competition between Condensation and Coagulation

Kieudiem Nguyen¹, Meredith Schervish¹, Pascale S. J. Lakey¹, James N. Smith¹, Manabu Shiraiwa^{1,*}

¹ Department of Chemistry, University of California, Irvine, USA

* m.shiraiwa@uci.edu

7 Abstract

The evolution of particle size distribution of secondary organic aerosols (SOA) is influenced by condensation and coagulation. Amorphous semisolid and glassy states in SOA cause kinetic limitations for condensational growth, but the impact of these phase states on the competition between condensation and coagulation has not been evaluated. In this work, we implement coagulation into the kinetic multilayer model of gas-particle interactions (KM-GAP) to calculate timescales of SOA partitioning and coagulation for liquid, semisolid, and highly viscous particles for closed and open systems. We find that the phase state may not have major impacts on coagulation timescale, with particle size playing a more critical role. The equilibration timescale of SOA partitioning is shorter than the coagulation timescale for most conditions in the closed system, while coagulation becomes competitive especially for high particle number concentration and highly viscous phase state ($D_b \le 10^{-15} \text{ cm}^2 \text{ s}^{-1}$) due to prolonged timescale of partitioning. We also illustrate that coagulation is less significant for the growth of seed particles in chamber experiments even for viscous particles, as the condensation sink of low volatility compounds would be larger than the coagulation sink due to their efficient mass accommodation. Coagulation becomes important during nanoparticle growth and the interplay between condensation and coagulation can result in the emergence of a bimodal size distribution with nanoparticles likely adopting a low viscosity phase state. Coagulation is also important for size distribution dynamics in a smoke plume for highly viscous submicron particles as their evaporation and condensation are inhibited with kinetic limitations.

Environmental significance:

The competition of condensation and coagulation is important in determining the evolution of particle size distribution and potential of nanoparticles to grow to cloud condensation nuclei. For particles with low viscosity, condensation tends to dominate and grow particles efficiently.

- 31 Coagulation becomes a competitive process for highly viscous particles, modulating particle size
- 32 distribution dynamics especially during new particle formation and biomass burning plumes with
- 33 high particle number concentrations.

Introduction

Secondary organic aerosols (SOA) are ubiquitous in the atmosphere, accounting for a large fraction of submicron particles. They impact climate, air quality, and public health. SOA are generated through oxidation of volatile organic compounds (VOCs) emitted from anthropogenic and biogenic sources to form semi-volatile and low-volatile organic compounds, which can subsequently condense into preexisting particles. The size of an SOA particle affects how it scatters and absorbs incoming solar radiation, as well as its ability to form clouds, influencing the Earth's radiation and climate. When the nanoparticles grow to ~100 nm in diameter, they can potentially serve as cloud condensation nuclei (CCN). The growth and survival of nanoparticles to CCN-relevant sizes are governed by the competing dynamic processes of condensation growth and coagulation loss. The condensation process involves a series of mass transport processes including gas-phase diffusion, gas-surface transfer, surface-bulk exchange, and bulk diffusion within the particle. These processes are often represented as fast relative to the timescales of other atmospheric processes, as SOA particles were traditionally assumed to be homogeneous and quasi-liquid droplets.

Laboratory experiments and atmospheric measurements have demonstrated SOA particles can adopt liquid (dynamic viscosity $\eta \leq 10^2$ Pa s), semi-solid ($10^2 \leq \eta \leq 10^{12}$ Pa s), or glassy ($\eta \geq 10^{12}$ Pa s) states, depending on chemical composition, relative humidity, and temperature. ¹²⁻¹⁴ Global and regional modeling studies suggested that SOA particles exist in an amorphous solid or glassy state in the free troposphere and over deserts with low relative hudmidity. ¹⁵⁻²⁰ This can lead to prolonged characteristic bulk diffusion timescales of organic molecules within SOA particles ^{21, 22} and facilitate long-range transport of toxic organic compounds in the atmosphere. ^{23, 24} Modeling studies also demonstrated that partitioning of semi-volatile compounds into highly viscous aerosols leads to kinetically-limited growth with prolonged equilibration timescales of SOA partitioning ²⁵ and particle-particle mixing timescales ^{26, 27} thus affecting the evolution of particle size distributions upon SOA growth. ²⁸⁻³³

Coagulation is a kinetic process in which two particles collide and stick together to form a larger particle. Coagulation reduces the number of particles while conserving the particle volume concentration. Chamber and flow tube experiments often reduce the impact of coagulation by keeping the particle concentration low or short residence times; Al-36 however, particle concentrations cannot be controlled in new particle formation chamber experiments, so it is important to account for coagulation. This drives the need to better understand how particle phase state impacts the interplay of condensation and coagulation, which determines the evolution of particle size distributions.

In this study, we apply the kinetic multilayer model of gas-particle interactions in aerosols and clouds (KM-GAP)^{28, 37} to investigate the timescales of condensation and coagulation of aerosols under the combined impacts of particle phase state and volatility of condensing species. We simulate the evolution of particle size distribution to illustrate the competition of condensation and coagulation in laboratory chamber experiments of growth of SOA and freshly nucleated particles as well as the evolution of particle size distribution in a biomass burning plume. The modeling results are compared with experimental and modeling studies for each scenario to provide a better understanding of the competition between condensation and coagulation.

Method

KM-GAP is used to simulate the evolution of particle size distribution by condensation and coagulation. KM-GAP consists of multiple model compartments and layers: a gas phase, a near-surface gas phase, a sorption layer, a near surface bulk layer, and ten bulk layers. The processes that are explicitly considered in KM-GAP are gas-phase diffusion, adsorption and desorption, surface-bulk exchange, and bulk diffusion. For size-resolved simulations, the bin method with a fully mobile size structure is used, in which the particle sizes change in each size bin due to condensation.

Coagulation has previously not been treated in KM-GAP. In this study, we implemented coagulation in KM-GAP by including Eq. (1), which describes the change in number concentration in particle size bin k (N_k , in cm⁻³) due to coagulation:^{38, 39}

$$\frac{dN_k(t)}{dt} = \frac{1}{2} \sum_{j=1}^k \left(\sum_{i=1}^k \frac{v_i + v_j}{v_k} f_{i,j,k} K_{i,j} N_i N_j \right) - N_k \sum_{j=1}^{N_{\text{bin}}} K_{k,j} N_j$$
(1)

where N_i and N_j are the number concentration of particles and v_i and v_j are the single particle volume in the size bin i and j (cm⁻³), respectively. $K_{i,j}$ is the Brownian coagulation coefficient (cm³ s⁻¹) for collision between particles in the size bin i and j (see Table S1 for calculation). N_{bin} is the number of size bins. The first term in Eq. (1) represents an increase of particle number concentration in the size bin k by coagulation of smaller particles and the second term accounts for coagulation loss of particles in the size bin k. To conserve mass concentration of particles upon coagulation, we apply $f_{i,j,k}$, which is the volume fraction of a coagulated pair i, j partitioned into bin k as calculated from:⁴⁰

$$f_{i,j,k} = \begin{cases} \left(\frac{v_{k+1} - V_{i,j}}{v_{k+1} - v_k}\right) \frac{v_k}{V_{i,j}}, & v_k \le V_{i,j} < v_{k+1}; k < N_{bin} \\ 1 - f_{i,j,k-1}, & v_{k-1} < V_{i,j} < v_k; k > 1 \\ 1, & V_{i,j} \ge v_k; k = N_{bin} \\ 0, & \text{all other cases} \end{cases}$$
 (2)

where $V_{i,j} = v_i + v_j$ is the total volume of coagulated particle from size i and j, having volume v_i and v_j respectively. This coagulated particle, which falls between volumes of two model size bins, k and k+1 with volume v_k and v_{k+1} , respectively, is partitioned in these two bins. We assumed that particles have the same chemical composition in each size bin, and they do not grow out of the largest size bin in the distribution after coagulation.

The model simulations are mainly conducted with a closed system, in which condensation of species would lead to a decrease in its gas phase mass concentration and an increase in its particle phase mass concentration. The closed system represents chamber experiments in a batch mode. Additional simulations with an open system with a fixed gas phase concentration were also conducted to represent chamber experiments with continuous flow and ambient conditions where the condensing species may be continuously generated. The surface accommodation coefficient is set to 1 based on molecular dynamics simulations.^{41, 42} We simulate different phase states of particles with typical bulk diffusivities $D_b = 10^{-8}$ cm² s⁻¹ for a liquid particle, $D_b = 10^{-15}$ cm² s⁻¹ for a semisolid particle, $D_b = 10^{-17}$ cm² s⁻¹ for a highly viscous particle. These diffusivities are chosen to represent a range found in atmospherically relevant aerosol particles.²¹ D_b is fixed at any given

depth in the particle bulk for each simulation, assuming condensation of semi-volatile compounds would not alter particle viscosity and diffusivity. We did not consider potential viscosity/diffusivity change, which is beyond the scope of this manuscript. The volatility, expressed as the pure compound saturation mass concentration (C^0) of condensing species, and the particle number concentration are also varied.

To examine how the competition between condensation and coagulation is affected by particle phase state, we evaluate the equilibration timescale of SOA partitioning (τ_{eq}) and characteristic coagulation timescale (τ_{coag}) by simulating condensation of species Z into pre-existing nonvolatile poly-dispersed particles. τ_{eq} is calculated as the e-folding time when the condensing species (Z) achieves equilibrium in the particle phase, which is the first time (t) at which following condition is satisfied:⁴³

$$\frac{|\mathcal{C}_{\mathbf{p}}(t) - \mathcal{C}_{\mathbf{p},\mathbf{eq}}|}{|\mathcal{C}_{\mathbf{p},0} - \mathcal{C}_{\mathbf{p},\mathbf{eq}}|} < \frac{1}{e} \tag{3}$$

where $C_{p,0}$, and $C_{p,eq}$ are the mass concentration of Z in the particle phase at initial condition and at equilibrium, respectively.

Following common practice, $\tau_{\rm coag}$ is defined as the time necessary for reduction of the initial particle number concentration to half its initial value.³⁸ For monodispersed and polydispersed particles, $\tau_{\rm coag}$ can be calculated numerically from the decrease of the total particle number concentration in KM-GAP simulations. Additionally, for monodisperse particles with particle diameter $D_{\rm p}$, self-coagulation timescale ($\tau_{\rm scoa}$) can be calculated analytically as follows:³⁸,

$$\tau_{\text{scoa}} = \frac{2}{KN_0} \tag{4}$$

where N_0 is initial particle number concentration and K is the coagulation coefficient. K is a function of particle diameter, Brownian diffusivity of a particle, mean thermal velocity of a particle, and coagulation efficiency (see Table S1 for equations). For derivation of Eq. (4), the coagulation coefficient is assumed to be constant for monodispersed particles. K is a function of coagulation efficiency (α), which represents a fraction of collisions that result in coagulation. Coagulation efficiency is size-dependent: it decreases as the particles get smaller and can decrease down to 0.1 for nanoparticles. ^{45, 46} Previous modeling studies have shown that coagulation efficiency of soot particles is much lower compared to similarly sized metal nanoparticles due to shallower attractive

forces upon collision.⁴⁷ This suggests that glassy viscous particles might exhibit a lower coagulation efficiency. Therefore, we calculated τ_{scoa} for monodisperse particles with coagulation efficiency of 1 and 0.1 to explore its influence on τ_{scoa} .

Fig. 1 shows τ_{scoa} for monodisperse particles as a function of particle diameter ($D_{\text{p}}=1$ nm $-10~\mu\text{m}$) and particle number concentrations ($N_0=10^3-10^8~\text{cm}^{-3}$) with α of 1 and 0.1. For both cases, higher N_0 leads to shorter τ_{scoa} as it increases the probability of two particles to collide and coagulate. For a given N_0 , coagulation is more efficient with shorter τ_{scoa} for D_{p} in the 10-100 nm size range due to their relatively high mobility leading to higher coagulation coefficient. When the coagulation efficiency is decreased to 0.1, τ_{scoa} of particles in the 1-10 nm size range increase an order of magnitude due to their small cross-sectional area, which reduces the probability of coagulation. τ_{scoa} of larger particles is slightly increased, but within an order of magnitude compared to τ_{scoa} with α of 1. It suggests that τ_{scoa} of larger particles is less sensitive to the changing collision efficiency. Nanoparticles ($D_{\text{p}} < 20~\text{nm}$) were observed to bounce less on an impactor τ_{m} and they tend to adopt a less viscous phase state due to the nanosized effect, which suppresses the glass transition temperature. τ_{m} Thus, the phase state may not have major impacts on the coagulation timescale, with particle size playing a more dominant role.

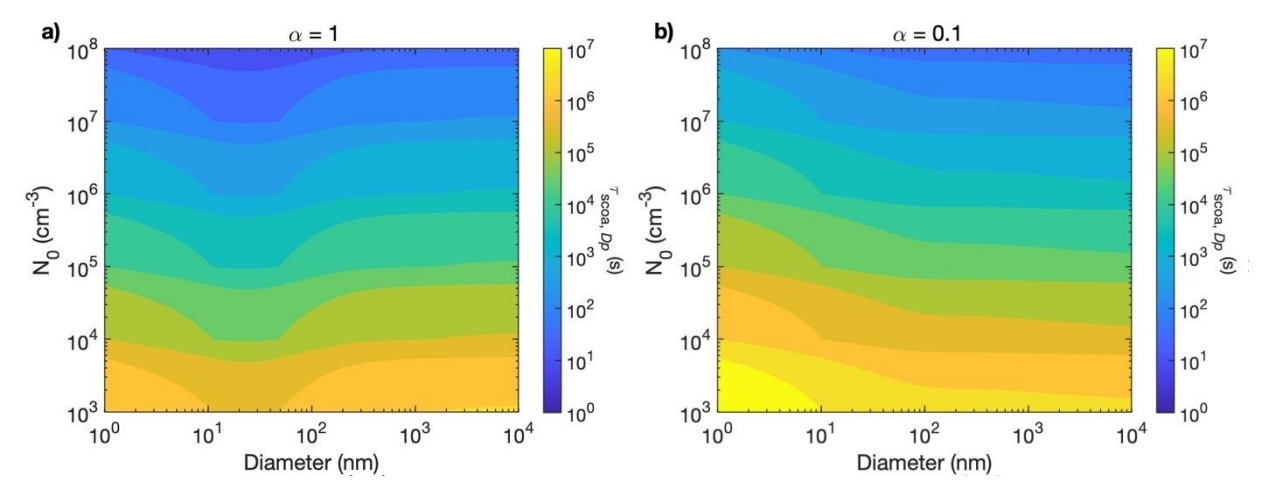


Fig. 1. Characteristic self-coagulation timescale (τ_{scoa}) for monodisperse particles as a function of particle diameter ($D_p = 1 \text{ nm} - 10 \text{ }\mu\text{m}$) and particle number concentrations ($N_0 = 10^3 - 10^8 \text{ cm}^{-3}$) with different coagulation efficiencies: (a) $\alpha = 1$, (b) $\alpha = 0.1$.

In order to compare condensation and coagulation scavenging rates for a specific size of particles, we calculate the timescales of coagulation ($\tau_{\text{coag},i}$) and condensation ($\tau_{\text{cond},i}$). The removal

160

161

162

163

164

165

166

167

168

169

170

171

172

173

174

175

176

timescale of particles in the size bin *i* due to coagulation with other particles is the inverse of the coagulation sink for a specific size which determines the amount of time for the particles in size bin *i* to be removed through coagulation:⁵¹

$$\tau_{\text{coag},i} = \frac{1}{\text{CoagSink}_i} = \frac{1}{\sum_{j=1}^{\text{Nbin}} K_{i,j} N_j}$$
 (5)

where $K_{i,j}$ is the coagulation coefficient between particle size i and j. N_j is the particle number concentration in the size bin j.

The condensation timescale (τ_{cond}) is the inverse of the condensation sink, which determines the loss of vapors onto surfaces of the existing particles:^{44, 51}

$$\tau_{\text{cond},i} = \frac{1}{\text{CS}_i} = \frac{1}{2\pi D_q D_{p,i} \beta (K n_i, \alpha_{\text{eff},i}) N_i}$$
(6)

where D_g is the gas-phase diffusion (cm² s⁻¹), $D_{p,i}$ and N_i is the particle diameter and number concentration in the size bin i. $\beta(Kn_i,\alpha_{\mathrm{eff},i})$ is the transition regime correction factor which is dependent on particle Knudsen number (Kn) and effective mass accommodation coefficient $(\alpha_{\mathrm{eff},i})$. $\alpha_{\mathrm{eff},i}$ is the probability of a gas molecule colliding with the surface to effectively enter the particle bulk, which can be calculated by accounting for kinetic limitations of bulk diffusion:⁵²

$$\alpha_{\text{eff},i} = \alpha_{\text{s}} \frac{1}{1 + (\frac{\alpha_{\text{s}}\omega C^{0}}{4D_{\text{p}}\rho_{\text{p}}}) \frac{r_{\text{p},i}}{5} \times 10^{-12}}$$
(7)

where α_s is surface accommodation coefficient assumed to be 1, ω is the mean thermal velocity (cm s⁻¹), C^0 is the pure compound saturation mass concentration of condensing species ($\mu g m^{-3}$), D_b is the particle bulk diffusivity (cm² s⁻¹), ρ_p is the particle density (g cm⁻³), and $r_{p,i}$ is the radius of particle size i (cm). $\alpha_{eff,i}$ provides an efficient way of accounting for bulk diffusivity so that τ_{cond} considers the effect of particle phase state and size on SOA partitioning. Note that τ_{cond} is different from τ_{eq} , which represents the e-folding time for condensing species to achieve equilibrium with the total particle population. τ_{cond} represents the timescale of growth of particles with a specific size via condensation.

Results and discussion

178

179

180

181

182

183

184

We conducted KM-GAP simulations to investigate the competition of condensation and coagulation (τ_{eq} vs. τ_{coag}) on particle number concentrations and the volatility of the condensing species in the closed and open systems. Then we applied KM-GAP to explore the influence of particle phase state on the competition between condensation and coagulation by simulating the growth of particles in chamber experiments and in biomass burning plumes. It is important to note that the aim of this study is not to reproduce the experimental results, but rather to simulate exemplary conditions to probe the interplay and competition of condensation and coagulation.

Equilibration timescales of SOA partitioning (τ_{eq}) vs. Coagulation timescales (τ_{coag})

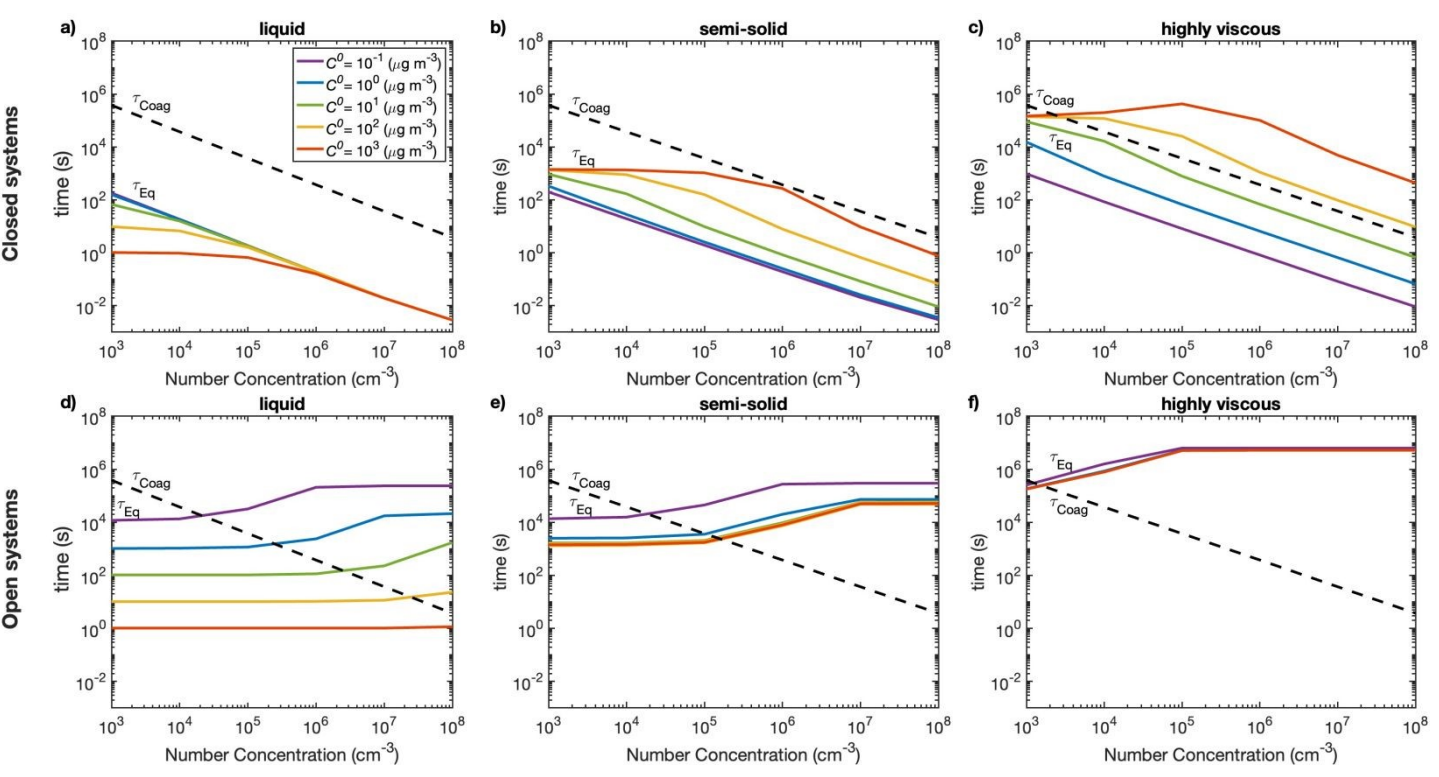


Fig. 2. Equilibration timescales of SOA partitioning (τ_{eq} , green lines) and coagulation timescales (τ_{coag} , black dashed line) as a function of particle number concentration ($10^3 - 10^8$ cm⁻³) for (a, d) liquid with bulk diffusivity $D_b = 10^{-8}$ cm² s⁻¹, (b, e) semisolid with $D_b = 10^{-15}$ cm² s⁻¹, and (c, f) highly viscous particles $D_b = 10^{-17}$ cm² s⁻¹. The top panels represent the closed system, while bottom panels are for the open system. τ_{eq} was calculated for species with different volatilities ($C^0 = 10^{-1} - 10^3$ μg m⁻³), getting lighter in color from low to higher volatilities.

In this section, the competition between condensation and coagulation is investigated for a system consisting of pre-existing seed particles and a condensing vapor. Specifically, the model simulates the condensation of semi-volatile species with pure compound saturation mass concentration of $C^0 = 10^{-1} - 10^3 \, \mu g \, \text{m}^{-3}$ into pre-existing non-volatile particles with initially lognormal size distribution with the mean diameter of 100 nm and geometric standard deviation of 0.3. The particle phase state is assumed to be liquid with $D_b = 10^{-8} \, \text{cm}^2 \, \text{s}^{-1}$, semi-solid with $D_b = 10^{-15} \, \text{cm}^2 \, \text{s}^{-1}$ and highly viscous with $D_b = 10^{-17} \, \text{cm}^2 \, \text{s}^{-1}$. We assume instantaneous coalescence with coagulation efficiency of 1 for all cases. The initial gas-phase mass concentration of condensing species is set at $10^{-2} \, \mu g \, \text{m}^{-3}$. The condensing species is assumed to have a molar mass of 200 g mol⁻¹ and density of 1.4 g cm⁻³, which are assumed to be the same for non-volatile species. The particle number concentration varies from $10^3 \, \text{to} \, 10^8 \, \text{cm}^{-3}$ which covers particle concentrations from suburban clean environments to heavily polluted areas in megacities. The simulations are conducted for both closed and open systems at 298K and 1 atm. The parameters are summarized in Table S2.

Fig. 2 shows the simulated $\tau_{\rm eq}$ (solid green lines) and $\tau_{\rm coag}$ (black dashed lines) as a function of particle number concentration ($N_{\rm p}$). $\tau_{\rm coag}$ decreases from $\sim 10^6$ s at $N_{\rm p} = 10^3$ cm⁻³ to ~ 10 s at $N_{\rm p} = 10^8$ cm⁻³ and it is independent of the volatilities of condensing species. $\tau_{\rm eq}$ varies from seconds to months depending on particle concentrations, the volatility of the condensing species, and the particle phase state. ^{43,55} When the particle is liquid ($D_{\rm b} = 10^{-8}$ cm² s⁻¹) in the closed system (Fig. 2a), $\tau_{\rm eq}$ is $<\sim 100$ s, depending mainly on $N_{\rm p}$. Higher $N_{\rm p}$ means higher surface concentration, resulting in higher condensation sink and a shorter $\tau_{\rm eq}$. When $N_{\rm p} > 10^6$ cm⁻³, condensation is limited by gas diffusion and accommodation; hence, $\tau_{\rm eq}$ does not depend on the volatility of the condensing species. When $N_{\rm p} < 10^6$ cm⁻³, $\tau_{\rm eq}$ is influenced by the volatility of the condensing species: $\tau_{\rm eq}$ is shorter with higher C^0 as only small amounts need to partition to reach equilibrium, while $\tau_{\rm eq}$ is longer with lower C^0 as more mass needs to be transported from the gas to particle phase. Overall, condensation is a dominant process over coagulation as $\tau_{\rm eq}$ is always shorter than $\tau_{\rm coag}$ for liquid particles in the closed system.

When the particle is semi-solid with $D_b = 10^{-15}$ cm² s⁻¹, τ_{eq} is longer compared to liquid particles due to kinetic limitations of bulk diffusion, but still shorter than τ_{coag} (Fig. 2b). The opposite trend in volatility is found for τ_{eq} , which is shorter for lower volatility compounds. This

216

217

218

219

220

221

222

223

224

225

226

227

228

229

230

231

232

233

234

235

236

237

238

239

240

241

242

243

244

is consistent with previous work on the effect of volatility on the equilibration timescales in a closed system. $^{25, 43}$ For compounds with higher C^0 , re-evaporation from semi-solid particles is significant due to slow surface-bulk exchange and bulk diffusion, leading to an increase in τ_{eq} . τ_{eq} is shorter for compounds with lower C^0 in absence of re-evaporation due to their low volatility nature, leading to a faster establishment of local thermodynamic equilibrium between the gasphase and near-surface bulk. $^{6, 56}$ As shown in Fig. 2c, τ_{eq} becomes an order of magnitude longer when the particle is highly viscous with $D_b = 10^{-17}$ cm² s⁻¹ compared to semi-solid. For semivolatile compounds with $C^0 \ge 10^2 \,\mu \text{g m}^{-3}$, τ_{eq} is longer than τ_{coag} , indicating that coagulation is a competitive process with condensation. Nevertheless, condensation is a dominant process over coagulation for most conditions in the closed system.

In the open system, τ_{eq} becomes significantly longer as more mass must be transported from the gas to particle phase, as also demonstrated by previous modeling studies. 25, 43, 57 τ_{eq} is longer with higher $N_{\rm p}$ with higher absorbing mass. For liquid particles with $D_{\rm b} = 10^{-8}~{\rm cm^2~s^{-1}},~\tau_{\rm eq}$ for semi-volatile compounds is still shorter than τ_{coag} (Fig. 2d). τ_{eq} of low-volatile compounds become longer than τ_{coag} especially at high N_{p} . τ_{eq} for semi-solid (Fig. 2e) and highly viscous particles (Fig. 2f) is less sensitive to C^0 because the timescale to achieve equilibrium is primarily controlled by bulk diffusion. In these cases, coagulation plays an increasingly significant role when the timescale for achieving equilibrium is extended due to bulk diffusion limitations. While condensation of low-volatile organic compounds (LVOCs) continues to occur, the prolonged equilibration allows coagulation to become competitive, especially for highly viscous phase state and high particle number concentration.

Growth of SOA in chamber experiments

We simulated the growth of SOA from oxidation products of α -pinene ozonolysis in the presence of seed particles, which have been widely studied in chamber experiments.^{58, 59} The initial size distribution of non-volatile seed particles was assumed with the mean diameter of 100 nm and particle number concentration of 4×10³ cm⁻³ and 2×10⁴ cm⁻³, which correspond to seed mass concentration of 5 μg m⁻³ and 20 μg m⁻³, respectively.⁵⁹ The initial gas-phase concentration of αpinene ($C^0 = 10^7 \,\mu\text{g m}^{-3}$) was set to be 50 $\,\mu\text{g m}^{-3}$, corresponding to 9 ppb at 1 atm and 298 K. For simplicity, we consider two products with semi-volatile (SVOC; $C^0 = 1 \mu \text{g m}^{-3}$) and low-volatile organic compounds (LVOC; $C^0 = 10^{-2} \,\mu\text{g m}^{-3}$). The gas-phase yields from α -pinene ozonolysis for

246

247

248

249

250

SVOC and LVOC were assumed as 0.3 and 0.14, respectively, based on a previous study.⁶⁰ The second-order rate constant of α -pinene and ozone is set to be 8×10^{-17} cm³ s⁻¹.⁶¹ Particle-phase reactions are not considered as we aim to focus on the particle growth primarily driven by condensable vapor and coagulation. The effect of phase state is considered with different bulk diffusivities ($D_b = 10^{-8}$, 10^{-15} , 10^{-18} cm² s⁻¹). Losses of particles and vapors on walls are not treated for simplicity.

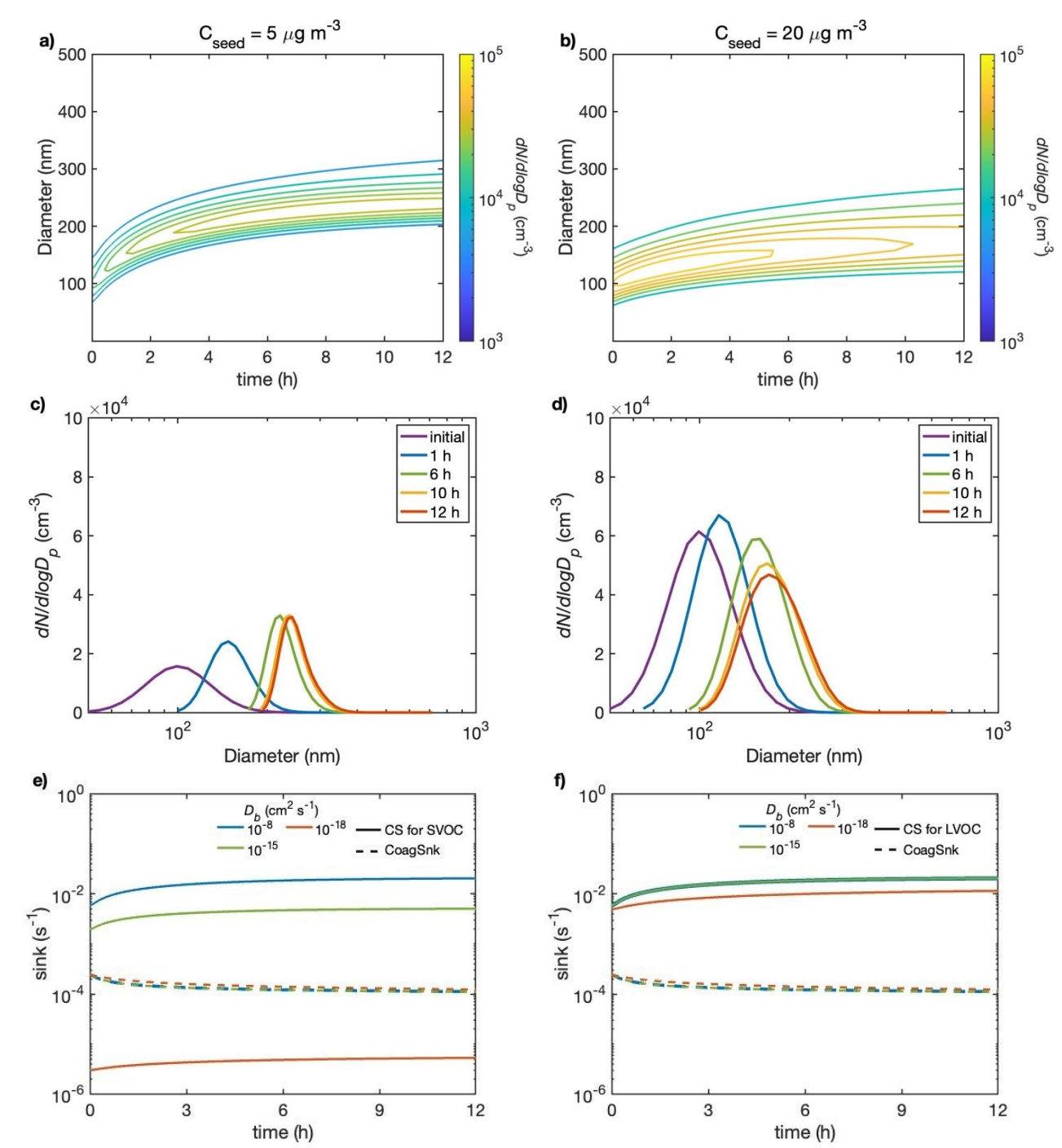


Fig. 3. Modeled evolution of particle number-size distribution in (a, b) contour plots and (c, d) $dN/d\log D_p$ at different times for SOA growth in chamber experiments for semi-solid particles (D_b = 10^{-15} cm² s⁻¹) with initial seed mass concentration of (a, c) 5 μg m⁻³ ($N_p = 4 \times 10^3$ cm⁻³) and (b, d) 20 μg m⁻³ ($N_p = 2 \times 10^4$ cm⁻³). Coagulation sink (CoagSnk, dashed lines) and condensation sink (CS, solid lines) for (e) SVOC and (f) LVOC calculated for the initial seed concentrations of 5 μg m⁻³ and bulk diffusivities of 10^{-8} , 10^{-15} and 10^{-18} cm² s⁻¹.

Fig. 3 shows the evolution of particle number size distribution for semi-solid particles ($D_b = 10^{-15} \text{ cm}^2 \text{ s}^{-1}$) with initial seed mass concentration of (a, c) 5 µg m⁻³ ($N_p = 4 \times 10^3 \text{ cm}^{-3}$) and (b, d) 20 µg m⁻³ ($N_p = 2 \times 10^4 \text{ cm}^{-3}$), showing that the particle mean diameter increases from 100 nm to ~240 nm and ~170 nm, respectively, in 12 hours. For seed mass concentrations of 5 µg m⁻³, the modeled size distribution narrows in the first hours, which is characteristic for gas-phase diffusion limited condensational growth.⁶² As the condensable vapor concentration decreases, the size distribution shifts slightly toward larger sizes with slow condensation after 6 h. This continuous growth in particle size suggests that condensation is a dominant process over coagulation. In contrast, at a higher seed concentration of 20 µg m⁻³, the modeled number size distribution initially narrows in the first hour but subsequently broadens, associated with reduction of particle number concentration after 6 h. This indicates that coagulation becomes important prominently impacting the size distribution due to high particle concentrations favoring coagulation. A similar behavior is observed in the case of liquid particles ($D_b = 10^{-8} \text{ cm}^2 \text{ s}^{-1}$), as shown in Fig. S1.

To investigate the effect of seed particle diameters, we conducted simulations with initial seed mean diameter of 200 nm with number concentrations of 5×10^3 cm⁻³ corresponding to 50 µg m⁻³.63 The model simulation in Fig. S2 shows that SOA particles grow to ~300 nm in 6 h with a narrowing of the characteristic in size distribution, indicating the dominance of condensation. Afterwards, particles grow only slightly with a broadening of the size distribution and a slight reduction of N_p , exhibiting minor contributions from coagulation. The comparison of results of Fig. 2 and Fig. S2 emphasizes the importance of the particle size and number concentration. The coagulation coefficient is smaller for large seed particle size, leading to longer coagulation timescales (e.g., Fig. 1).

The effect of phase state is further investigated by simulating SOA growth with different bulk diffusivities (10-8 (liquid), 10-15 (semi-solid) and 10-18 (ultra-viscous) cm² s⁻¹) and calculating

276

277

278

279

280

281

282

283

284

285

286

287

288

289

290

291

292

293

294

295

296

297

298

299

300

301

302

coagulation sink (CoagSnk) and condensation sink (CS) for SVOC (Fig. 3e) and LVOC (Fig. 3f). Coagulation sink is initially $\sim 2 \times 10^{-4}$ s⁻¹ and decreases slightly to $\sim 10^{-4}$ s⁻¹ over 12 hours. It is mostly independent of bulk diffusivity, as coagulation is not affected by particle phase state (coagulation efficiency of 1 is assumed for all cases). In contrast, the condensation sink for SVOC depends strongly on bulk diffusivity, being the highest at $\sim 10^{-2}$ s⁻¹ for liquid, $\sim 2 \times 10^{-3}$ s⁻¹ for semisolid, and ~3×10⁻⁶ s⁻¹ for ultra-viscous phase state. This is because the effective mass accommodation coefficient (α_{eff}) is reduced due to kinetic limitations in viscous phase states. For LVOCs, the condensation sink is $\sim 10^{-2}$ s⁻¹ for all phase states, as $\alpha_{\rm eff}$ remains close to unity due to LVOCs ability to condense effectively irrespective of the phase state.⁵² For liquid and semi-solid states, the condensation sink of SVOC and LVOC are both higher than the coagulation sink, confirming that condensation dominates over coagulation. For the ultra-viscous state, the coagulation sink is larger than the condensation sink of SVOC but lower than that of LVOC, indicating that condensation of SVOC is suppressed but condensation of LVOC is still the dominant process. These simulations suggest at low aerosol number concentrations, it is reasonable to assume coagulation has a negligible impact on the overall size distribution. However, in conditions of high particle concentrations, coagulation should be considered for accurate evaluation of particle size distribution as coagulation loss becomes significant (Fig. S3).

Growth of freshly nucleated particles

Freshly nucleated particles can grow via condensation, but they can be lost via coagulation. ^{51, 64} To investigate this competition in nanoparticle growth, we simulate the growth of freshly nucleated particles in the closed system. We referred to the Cosmics Leaving OUtdoor Droplets (CLOUD) experiments⁶⁵ to inform operating conditions of the experiments. An initial size distribution with the mean diameter of 2 nm was assumed with particle number concentration of 10^5 cm⁻³.⁶⁶ For simplicity, the simulation considers one condensing species, highly oxygenated organic molecules (HOMs) with low volatility ($C^0 = 10^{-4} \,\mu g \, m^{-3}$) at 263K, which has been shown to facilitate the initial growth of freshly nucleated particles.^{6, 67, 68} The mass concentrations of HOMs are set at 0.3 $\,\mu g \, m^{-3}$.⁶⁶ The effect of phase state is considered with different bulk diffusivities ($D_b = 10^{-8}$, 10^{-15} and 10^{-18} cm² s⁻¹)

304

305

306

307

308

309

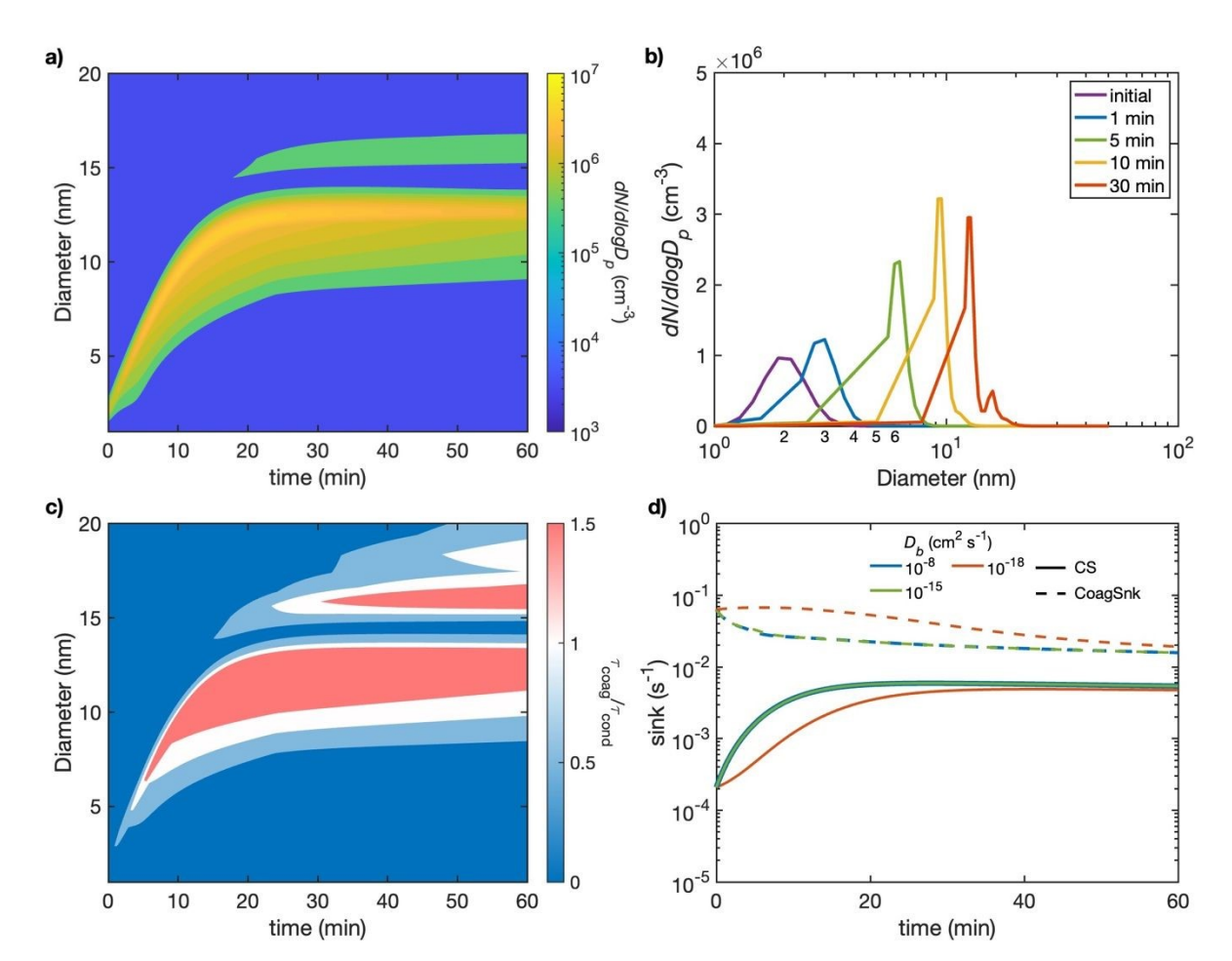


Fig. 4. Modeled evolution of particle number size distribution in (a) contour plot, (b) $dN/dlogD_p$ at different times for the growth of freshly nucleated particles with liquid particles ($D_b = 10^{-8}$ cm² s⁻¹). (c) Ratio of coagulation timescale to condensation timescale ($\frac{\tau_{coag}}{\tau_{cond}}$). Blue color means $\tau_{coag} < \tau_{cond}$, indicating coagulation is favored; red color means $\tau_{coag} > \tau_{cond}$, indicating condensation is favored. (d) Condensation sink (CS, solid lines) and coagulation sink (CoagSnk, dashed lines) calculated with $N_p = 10^5$ cm⁻³ and bulk diffusivities ranging from 10^{-8} to 10^{-18} cm² s⁻¹.

Fig. 4(a, b) shows the evolution of particle number size distribution for a liquid particle $(D_b = 10^{-8} \text{ cm}^2 \text{ s}^{-1})$. In the first ten minutes, particles grow quickly to 10 nm due to rapid condensation of HOMs with the modeled number-size distribution exhibiting the narrowing characteristic of gas-phase diffusion limited growth. The particle diameter reaches ~13 nm after 20 min. As the concentration of HOMs decreases further, the peak of the size distribution begins to decrease and stays constant afterwards. There is a local minimum around 14 nm where particles are scavenged efficiently by larger particles, while condensational growth is not yet sufficient to

311

312

313

314

315

316

317

318

319

320

321

322

323

324

325

326

327

328

329

330

331

332

333334

335

336

337

338

339

340

grow this size. After 30 min, a second peak emerges at 16 nm. This bimodal size distribution is indeed observed in continuous flow chamber and CLOUD experiments. ^{66, 69, 70} The formation of a bimodal size distribution requires the interplay between condensation and coagulation, as condensation alone cannot form the observed bimodal distribution (see Fig. S4 for simulation without coagulation).

This is further demonstrated in Fig. 4c, showing the ratio of coagulation timescale to condensation timescale $(\frac{\tau_{\rm coag}}{\tau_{\rm cond}})$ for liquid particles ($D_{\rm b}$ = 10⁻⁸ cm² s⁻¹). Initially, $\tau_{\rm cond}$ is longer than $\tau_{\rm coag}$ for ultrafine particles ($D_{\rm p}$ < 5 nm) as shown in blue color (Fig. 4c), indicating that coagulation proceeds faster than condensation. The condensation of LVOCs to tiny particles is suppressed due to the Kelvin effect. These particles are highly vulnerable to self-coagulation and coagulation scavenging with larger particles. As a result, many freshly nucleated particles are likely lost before condensation can accelerate their growth, reducing the overall number concentrations of these particles. Once the particles increase in size, the Kelvin effect is reduced thus facilitating condensation of LVOCs. The appearance of a second mode is caused by coagulation growth of larger particles by scavenging smaller particles. Afterwards, condensation becomes increasingly important, as τ_{cond} becomes shorter than τ_{coag} (red area in Fig. 4c). Note that another possible explanation for the observed bimodal distribution for the CLOUD experiments is the rapid cocondensation of nitric acid and ammonia only after the particles reached $D_p \approx 4.6$ nm, ⁷⁰ which was not considered in our model simulations. Rapid growth from nitric acid and ammonia condensation could be fast enough to make the freshly nucleated particles less vulnerable to scavenging, thereby increasing their survival probability.

Fig. 4(d) shows condensation sink (CS) and coagulation sink (CoagSnk) for simulations with different bulk diffusivities (10⁻⁸ (liquid), 10⁻¹⁵ (semi-solid) and 10⁻¹⁸ (ultra-viscous) cm² s⁻¹). For all cases, CoagSnk is larger than CS, indicating that coagulation dominates over condensation. This is especially the case during early times, when CS is more than two orders of magnitude lower than CoagSnk. This gap becomes smaller upon growth of nanoparticles to larger sizes allowing CS to become larger; then condensation becomes a competitive process with coagulation. It is important to note that CS and CoagSnk are calculated for the total particle size distribution, rather than for specific particle sizes. Condensation and coagulation may not impact all particles with different size equally; particles with certain size ranges may experience more significant grow via condensation, while others may be vulnerable to coagulation.

CS and CoagSnk behave almost the same for liquid and semisolid particles. For ultraviscous particles, CoagSnk stays high, and CS increases more slowly due to strong kinetic limitations. In this case, nanoparticles grow slowly, and the formation of bimodal distribution was not observed in the simulations. These results are not consistent with laboratory observations, implying that freshly formed nucleated particles are more likely to adopt liquid or less-viscous phase state. This behavior is consistent with previous experimental findings, which demonstrated that freshly nucleated in sub 30 nm size range do not exhibit bounce properties due to differences in chemical composition and phase state compared to larger particles.⁴⁸ Cheng et al. (2015) has suggested that SOA particles at room temperature are expected to be always liquid at diameters below 20 nm due to the nanosized effect.⁷¹ Recent studies have shown that the glass transition temperature can be suppressed substantially upon a decrease of the particle size.^{49,50} These implied very small particles ($D_p < 20$ nm) maintain a low viscous phase state, facilitating the interplay between condensation and coagulation that results in the formation of bimodal size distribution observed in CLOUD chamber experiments. These results emphasize the importance of considering particle phase state when modeling nucleation and its subsequent growth.

Growth of biomass burning aerosol

To investigate the effect of phase state on the growth of biomass burning organic aerosols (BBOA), we simulate the temporal evolution of particle number size distribution in fresh smoke in biomass burning plumes with high particle number concentrations. Polydisperse particles with a mean diameter of 130 nm are modeled with $N_p = 3 \times 10^4$ cm⁻³ to represent fresh smoke biomass-burning observations. Page 320 contains semi-volatile organic compounds (SVOCs), which may evaporate and cause a reduction in particle mass. Page 40 consider particle population containing SVOC with $C^0 = 1 \mu \text{g m}^{-3}$. The model assumes an open system in which the SVOC concentration in the gas phase is fixed at 0.1, 1, or 10 $\mu \text{g m}^{-3}$ at 298 K to represent a range of concentrations of condensing species, respectively. BBOA can have a wide range of viscosity over a range of relative humidity, so we simulate with different bulk diffusivities ($D_b = 10^{-8}$, 10^{-15} , 10^{-18} cm² s⁻¹). Page 50 These simulations allow the evaluation of the influence of particle phase state on growth dynamics of BBOA. Note that we do not attempt to simulate any specific previously observed biomass burning plumes; instead, we simulate exemplary plume cases that undergo competition among condensation, evaporation and coagulation.

372

373

374

375

376

377

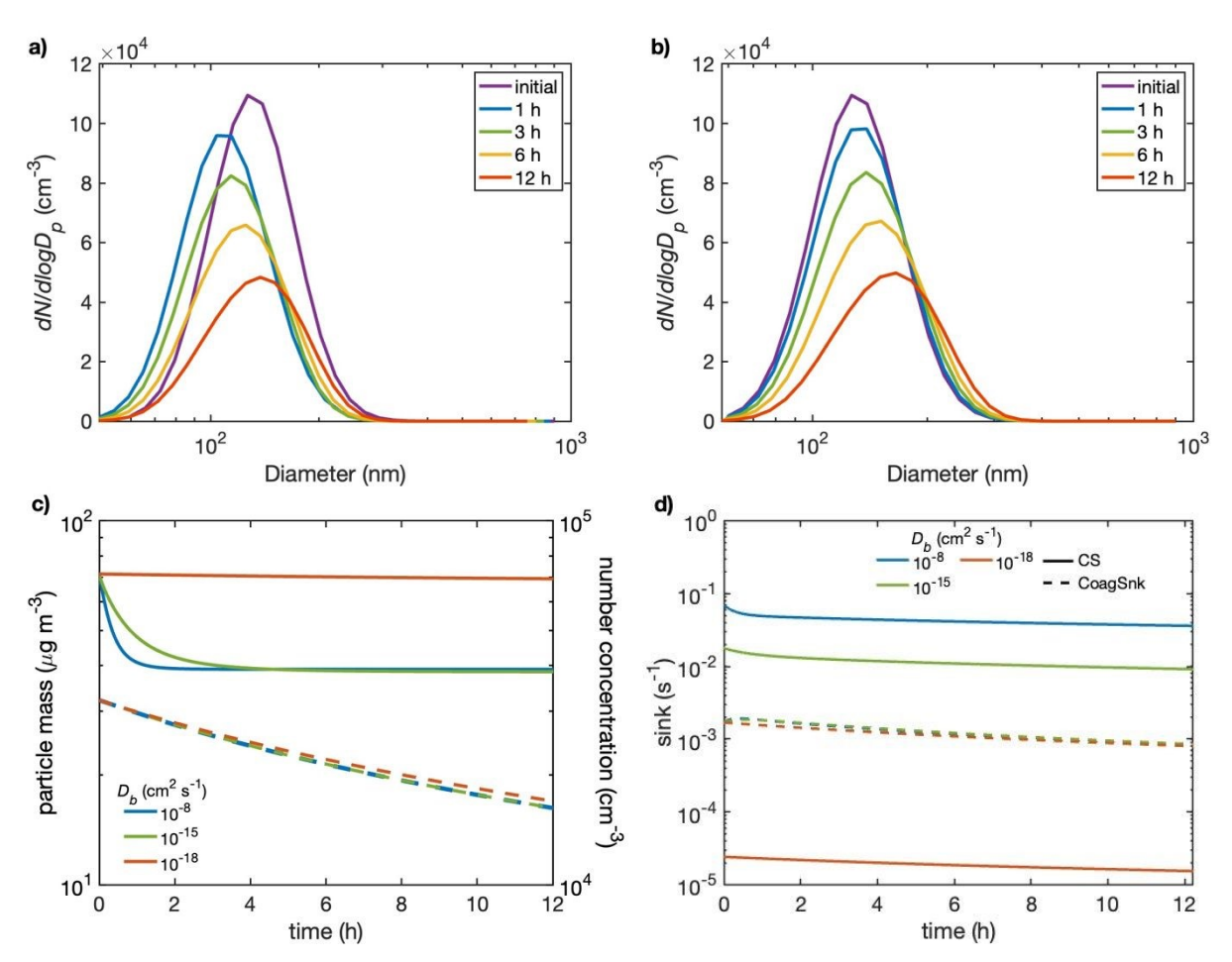


Fig. 5. Modeled number size distribution for the growth of biomass burning organic aerosols with (a) liquid particles ($D_b = 10^{-8}$ cm² s⁻¹) and (b) ultra-viscous particles ($D_b = 10^{-18}$ cm² s⁻¹) with SVOC concentration of 0.1 μg m⁻³. (c) Temporal evolution of particle mass concentration (solid lines, left axis) and particle number concentration (dashed lines, right axis). (d) Condensation sink (CS, solid lines) and coagulation sink (CoagSnk, dashed lines) calculated with bulk diffusivities of 10^{-8} , 10^{-15} , and 10^{-18} cm² s⁻¹.

Figure 5 shows the modeled number size distribution for (a) liquid ($D_b = 10^{-8}$ cm² s⁻¹) and (b) ultra-viscous particles ($D_b = 10^{-18}$ cm² s⁻¹). For liquid particles, the particle mean diameter decreases from 130 nm to ~100 nm within the first hour driven by the evaporation of SVOC and then increases to ~140 nm over 12 hours. Similar behavior is observed for semi-solid particles (Fig. S5). Fig. 5c shows the particle growth associated with a reduction of the particle number concentration, indicating the major contribution of coagulation. Fig. 5d depicts coagulation (CoagSnk) and condensation sink (CS), showing that CS is larger than CoagSnk for liquid

particles. This indicates that condensation still plays an important role in particle growth, which is especially the case with a higher gas-phase SVOC concentration ($C_g = 1 \mu g \text{ m}^{-3}$) (Fig. S6). For ultra-viscous particles, the particle mean diameter increases from 130 nm to ~170 nm over 12 hours. Evaporation and condensation of SVOC are both strongly suppressed in viscous particles due to bulk diffusion limitations. CS becomes much smaller than CoagSnk, resulting in primary growth from coagulation. Even with high gas phase SVOC concentration of 10 $\mu g \text{ m}^{-3}$ (Fig. S7) or higher particle number concentration of $4 \times 10^5 \text{ cm}^{-3}$ (Fig. S8), the particle growth is driven primarily by coagulation. These simulations are consistent with previous studies, ^{72, 73, 75, 81} showing that coagulation is the dominant growth mechanism with evaporation and condensation having a relatively minor impact in the smoke plume for highly viscous particles.

These simulations provide useful insights into the competing processes in particle growth under different conditions. Biomass burning plumes are highly variable in term of the composition, particle properties, atmospheric condition which can significantly influence the relative importance of condensation, evaporation, and coagulation in particle growth. So, the conclusions drawn from these simulations are specific to the conditions modeled and may not fully capture the complexity of real-world biomass burning plumes.

Discussion and Outlook

We have made a few assumptions that may represent limitations of this study. When two particles coagulate, the resulting particle's composition is assumed to match the composition of the larger particle, even though the composition of two particles may be different. This may lead to an overestimation or underestimation of semi-volatile species in coagulated particles, potentially affecting τ_{eq} especially for highly viscous particles when coagulation is significant. Another assumption is instantaneous coagulation, even though coalescence of some particles can take longer time. Molecular dynamic simulations have shown that the deformation of the smaller particle dominates the coalescence process in liquid particles, while diffusion processes dominate coalescence process for solid particles, leading to the longer timescales for the coalescence process. In addition, theoretical calculations and experimental studies showed that viscous effects can retard coagulation rate by an order of magnitude. Power et al. (2013) observed the coalescence timescale of two aerosol particles that combine to form a spherical particle from 10^{-7} to 10^{5} s, depending on viscosity. Bell et al. (2017) also observed that solid semi-volatile coating

Open Access Article. Published on 14 nuvembre 2025. Downloaded on 19/11/2025 1:24:40.

can inhibit the coalescence of coagulating particles for over two days.⁸⁹ These studies suggest prolonged coalescence can delay coagulation timescale in highly viscous particles. Further model development is required to incorporate the coalescence process to provide more accurate representations of particle size evolution of highly viscous particles.

Nevertheless, our study demonstrates that the competition of condensation and coagulation is affected by the particle phase state. While the coagulation timescale may not be heavily influenced by the phase state, semisolid and ultra-viscous phase states can prolong equilibration timescales of semi-volatile species substantially. Our results show that condensation plays a dominant role in particle growth at low particle number concentrations for liquid and semi-solid particles, while coagulation can have a significant impact on the evolution of particle size distribution of highly viscous particles at high particle number concentrations. The interplay between condensation and coagulation becomes particularly critical in the growth of freshly nucleated particles, which can lead to the emergence of bimodal size distribution as observed in chamber experiments. This underlines the significant role of coagulation growth in the evolution of particle number size distributions during nanoparticle growth. Additionally, coagulation is the primary cause of growth of highly viscous biomass burning aerosols, where significant particle concentrations can favor coagulation over condensation.

Chamber, flow tube, and modeling studies often simplify the role of coagulation and neglect the competing timescales of condensation and coagulation. We show that this assumption is justified in the cases where the particle phase adopts a low viscous state with low particle concentrations. If the particle is highly viscous or solid, the diffusion of condensing species significantly hinders mass transport to the bulk, constraining condensation growth and shifting the growth dynamics to favor coagulation. In such cases, ignoring coagulation may lead to inaccurate prediction of the evolution of particle size distributions especially for new particle formation and biomass burning plumes. Proper consideration of the particle phase state is critical for accurate representation of particle size distributions.

Supporting Information:

The Supporting Information is available.

- 438 Acknowledgements. We acknowledge funding from U. S. National Science Foundation (AGS-
- 439 2246502) and U.S. Department of Energy (DE-SC0022139 and DE-SC0021208).
- 440 Conflict of interests. We declare no conflict of interests.

442 References

441

443

444

445

446

447

448

449

450

451

452

453 454

455

456

457

458

459

460 461

462

463

464

465

466

467

468

469

- 1. J. L. Jimenez, M. R. Canagaratna, N. M. Donahue, A. S. H. Prevot, Q. Zhang, J. H. Kroll, P. F. Decarlo, J. D. Allan, H. Coe, N. L. Ng, A. C. Aiken, K. S. Docherty, I. M. Ulbrich, A. P. Grieshop, A. L. Robinson, J. Duplissy, J. D. Smith, K. R. Wilson, V. A. Lanz, C. Hueglin, Y. L. Sun, J. Tian, A. Laaksonen, T. Raatikainen, J. Rautiainen, P. Vaattovaara, M. Ehn, M. Kulmala, J. M. Tomlinson, D. R. Collins, M. J. Cubison, J. Dunlea, J. A. Huffman, T. B. Onasch, M. R. Alfarra, P. I. Williams, K. Bower, Y. Kondo, J. Schneider, F. Drewnick, S. Borrmann, S. Weimer, K. Demerjian, D. Salcedo, L. Cottrell, R. Griffin, A. Takami, T. Miyoshi, S. Hatakeyama, A. Shimono, J. Y. Sun, Y. M. Zhang, K. Dzepina, J. R. Kimmel, D. Sueper, J. T. Jayne, S. C. Herndon, A. M. Trimborn, L. R. Williams, E. C. Wood, A. M. Middlebrook, C. E. Kolb, U. Baltensperger and D. R. Worsnop, Evolution of Organic Aerosols in the Atmosphere, Science, 2009, 326, 1525-1529.
- 2. U. Pöschl and M. Shiraiwa, Multiphase Chemistry at the Atmosphere–Biosphere Interface Influencing Climate and Public Health in the Anthropocene, Chemical Reviews, 2015, **115**, 4440-4475.
- 3. M. Shrivastava, C. D. Cappa, J. Fan, A. H. Goldstein, A. B. Guenther, J. L. Jimenez, C. Kuang, A. Laskin, S. T. Martin, N. L. Ng, T. Petaja, J. R. Pierce, P. J. Rasch, P. Roldin, J. H. Seinfeld, J. Shilling, J. N. Smith, J. A. Thornton, R. Volkamer, J. Wang, D. R. Worsnop, R. A. Zaveri, A. Zelenyuk and Q. Zhang, Recent advances in understanding secondary organic aerosol: Implications for global climate forcing, Reviews of Geophysics, 2017, 55, 509-559.
- 4. M. Kanakidou, J. H. Seinfeld, S. N. Pandis, I. Barnes, F. J. Dentener, M. C. Facchini, R. Van Dingenen, B. Ervens, A. Nenes, C. J. Nielsen, E. Swietlicki, J. P. Putaud, Y. Balkanski, S. Fuzzi, J. Horth, G. K. Moortgat, R. Winterhalter, C. E. L. Myhre, K. Tsigaridis, E. Vignati, E. G. Stephanou and J. Wilson, Organic aerosol and global climate modelling: a review, Atmospheric Chemistry and Physics, 2005, 5, 1053-1123.
- 5. P. J. Ziemann and R. Atkinson, Kinetics, products, and mechanisms of secondary organic aerosol formation, Chemical Society Reviews, 2012, 41, 6582.
- 471 J. Tröstl, W. K. Chuang, H. Gordon, M. Heinritzi, C. Yan, U. Molteni, L. Ahlm, C. 6. 472 Frege, F. Bianchi, R. Wagner, M. Simon, K. Lehtipalo, C. Williamson, J. S. Craven, J. 473 Duplissy, A. Adamov, J. Almeida, A.-K. Bernhammer, M. Breitenlechner, S. Brilke, A. 474 Dias, S. Ehrhart, R. C. Flagan, A. Franchin, C. Fuchs, R. Guida, M. Gysel, A. Hansel, C. R. Hoyle, T. Jokinen, H. Junninen, J. Kangasluoma, H. Keskinen, J. Kim, M. Krapf, A. 475 476 Kürten, A. Laaksonen, M. Lawler, M. Leiminger, S. Mathot, O. Möhler, T. Nieminen, A. Onnela, T. Petäjä, F. M. Piel, P. Miettinen, M. P. Rissanen, L. Rondo, N. Sarnela, S. 477 Schobesberger, K. Sengupta, M. Sipilä, J. N. Smith, G. Steiner, A. Tomè, A. Virtanen, A. 478 479 C. Wagner, E. Weingartner, D. Wimmer, P. M. Winkler, P. Ye, K. S. Carslaw, J. Curtius,
- 480 J. Dommen, J. Kirkby, M. Kulmala, I. Riipinen, D. R. Worsnop, N. M. Donahue and U.

497

498

- Baltensperger, The role of low-volatility organic compounds in initial particle growth in the atmosphere, *Nature*, 2016, **533**, 527-531.
- O. Boucher, D. Randall, P. Artaxo, C. Bretherton, G. Feingold and P. Forster, Climate
 Change 2013 The Physical Science Basis, 2014, DOI: 10.1017/cbo9781107415324.
- U. Dusek, G. P. Frank, L. Hildebrandt, J. Curtius, J. Schneider, S. Walter, D. Chand, F.
 Drewnick, S. Hings, D. Jung, S. Borrmann and M. O. Andreae, Size matters more than chemistry for cloud-nucleating ability of aerosol particles, *Science*, 2006, 312, 1375-1378.
- H. Vehkamäki and I. Riipinen, Thermodynamics and kinetics of atmospheric aerosol
 particle formation and growth, *Chemical Society Reviews*, 2012, 41, 5160-5173.
- M. Shiraiwa, T. Berkemeier, K. A. Schilling-Fahnestock, J. H. Seinfeld and U. Pöschl,
 Molecular corridors and kinetic regimes in the multiphase chemical evolution of
 secondary organic aerosol, *Atmospheric Chemistry and Physics*, 2014, 14, 8323-8341.
- J. F. Pankow, An absorption model of gas/particle partitioning of organic compounds in the atmosphere, *Atmospheric Environment*, 1994, **28**, 185-188.
 - 12. A. Virtanen, J. Joutsensaari, T. Koop, J. Kannosto, P. Yli-Pirilä, J. Leskinen, J. M. Mäkelä, J. K. Holopainen, U. Pöschl, M. Kulmala, D. R. Worsnop and A. Laaksonen, An amorphous solid state of biogenic secondary organic aerosol particles, *Nature*, 2010, **467**, 824-827.
- T. Koop, J. Bookhold, M. Shiraiwa and U. Pöschl, Glass transition and phase state of organic compounds: dependency on molecular properties and implications for secondary organic aerosols in the atmosphere, *Physical Chemistry Chemical Physics*, 2011, **13**, 19238.
- 504 14. J. P. Reid, A. K. Bertram, D. O. Topping, A. Laskin, S. T. Martin, M. D. Petters, F. D. Pope and G. Rovelli, The viscosity of atmospherically relevant organic particles, *Nature Communications*, 2018, **9**.
- 507 15. M. Shiraiwa, Y. Li, A. P. Tsimpidi, V. A. Karydis, T. Berkemeier, S. N. Pandis, J. Lelieveld, T. Koop and U. Pöschl, Global distribution of particle phase state in atmospheric secondary organic aerosols, *Nature Communications*, 2017, **8**, 15002.
- R. Luu, M. Schervish, N. A. June, S. E. O'Donnell, S. H. Jathar, J. R. Pierce and M.
 Shiraiwa, Global Simulations of Phase State and Equilibration Time Scales of Secondary
 Organic Aerosols with GEOS-Chem, ACS Earth and Space Chemistry, 2025, DOI:
 10.1021/acsearthspacechem.4c00281.
- Y. Li, A. G. Carlton and M. Shiraiwa, Diurnal and Seasonal Variations in the Phase State
 of Secondary Organic Aerosol Material over the Contiguous US Simulated in CMAQ,
 ACS Earth and Space Chemistry, 2021, 5, 1971-1982.
- R. Schmedding, Q. Z. Rasool, Y. Zhang, H. O. T. Pye, H. Zhang, Y. Chen, J. D. Surratt,
 F. D. Lopez-Hilfiker, J. A. Thornton, A. H. Goldstein and W. Vizuete, Predicting
 secondary organic aerosol phase state and viscosity and its effect on multiphase
 chemistry in a regional-scale air quality model, *Atmospheric Chemistry and Physics*,
 2020, 20, 8201-8225.
- 522 19. Z. Zhang, Y. Li, H. Ran, J. An, Y. Qu, W. Zhou, W. Xu, W. Hu, H. Xie, Z. Wang, Y. Sun and M. Shiraiwa, Simulated phase state and viscosity of secondary organic aerosols over China, *Atmospheric Chemistry and Physics*, 2024, **24**, 4809-4826.

544

- Q. Z. Rasool, M. Shrivastava, M. Octaviani, B. Zhao, B. Gaudet and Y. Liu, Modeling
 Volatility-Based Aerosol Phase State Predictions in the Amazon Rainforest, ACS Earth
 and Space Chemistry, 2021, 5, 2910-2924.
- 528 21. M. Shiraiwa, M. Ammann, T. Koop and U. Pöschl, Gas uptake and chemical aging of semisolid organic aerosol particles, *Proceedings of the National Academy of Sciences*, 530 2011, **108**, 11003-11008.
- A. M. Maclean, C. L. Butenhoff, J. W. Grayson, K. Barsanti, J. L. Jimenez and A. K.
 Bertram, Mixing times of organic molecules within secondary organic aerosol particles:
 a global planetary boundary layer perspective, *Atmospheric Chemistry and Physics*, 2017,
 17, 13037-13048.
- Q. Mu, M. Shiraiwa, M. Octaviani, N. Ma, A. Ding, H. Su, G. Lammel, U. Pöschl and Y.
 Cheng, Temperature effect on phase state and reactivity controls atmospheric multiphase
 chemistry and transport of PAHs, *Science Advances*, 2018, 4, eaap7314.
- M. Shrivastava, S. Lou, A. Zelenyuk, R. C. Easter, R. A. Corley, B. D. Thrall, P. J.
 Rasch, J. D. Fast, S. L. Massey Simonich, H. Shen and S. Tao, Global long-range transport and lung cancer risk from polycyclic aromatic hydrocarbons shielded by coatings of organic aerosol, *Proceedings of the National Academy of Sciences*, 2017, 114, 1246-1251.
 - 25. M. Schervish and M. Shiraiwa, Impact of phase state and non-ideal mixing on equilibration timescales of secondary organic aerosol partitioning, *Atmospheric Chemistry and Physics*, 2023, **23**, 221-233.
- M. Schervish, N. M. Donahue and M. Shiraiwa, Effects of volatility, viscosity, and non-ideality on particle–particle mixing timescales of secondary organic aerosols, *Aerosol Science and Technology*, 2024, 58, 411-426.
- Q. Ye, M. A. Upshur, E. S. Robinson, F. M. Geiger, R. C. Sullivan, R. J. Thomson and
 N. M. Donahue, Following Particle-Particle Mixing in Atmospheric Secondary Organic
 Aerosols by Using Isotopically Labeled Terpenes, *Chem*, 2018, 4, 318-333.
- M. Shiraiwa, L. D. Yee, K. A. Schilling, C. L. Loza, J. S. Craven, A. Zuend, P. J.
 Ziemann and J. H. Seinfeld, Size distribution dynamics reveal particle-phase chemistry in organic aerosol formation, *Proceedings of the National Academy of Sciences*, 2013, 110, 11746-11750.
- R. A. Zaveri, J. E. Shilling, A. Zelenyuk, J. Liu, D. M. Bell, E. L. D'Ambro, C. J. Gaston,
 J. A. Thornton, A. Laskin, P. Lin, J. Wilson, R. C. Easter, J. Wang, A. K. Bertram, S. T.
 Martin, J. H. Seinfeld and D. R. Worsnop, Growth Kinetics and Size Distribution
 Dynamics of Viscous Secondary Organic Aerosol, *Environmental Science & Environmental Science & Technology*, 2018, 52, 1191-1199.
- R. A. Zaveri, J. E. Shilling, A. Zelenyuk, M. A. Zawadowicz, K. Suski, S. China, D. M.
 Bell, D. Veghte and A. Laskin, Particle-Phase Diffusion Modulates Partitioning of
 Semivolatile Organic Compounds to Aged Secondary Organic Aerosol, *Environmental Science & Science*
- R. A. Zaveri, J. Wang, J. Fan, Y. Zhang, J. E. Shilling, A. Zelenyuk, F. Mei, R. Newsom, M. Pekour, J. Tomlinson, J. M. Comstock, M. Shrivastava, E. Fortner, L. A. T. Machado, P. Artaxo and S. T. Martin, Rapid growth of anthropogenic organic nanoparticles greatly alters cloud life cycle in the Amazon rainforest, *Science Advances*, 2022, 8.
- Y. He, A. Akherati, T. Nah, N. L. Ng, L. A. Garofalo, D. K. Farmer, M. Shiraiwa, R. A.
 Zaveri, C. D. Cappa, J. R. Pierce and S. H. Jathar, Particle Size Distribution Dynamics

583

584

585

586

587

588

589

590

591

592

593

594

595

596

- Can Help Constrain the Phase State of Secondary Organic Aerosol, *Environmental Science & Environmental* 572 Science & Technology, 2021, **55**, 1466-1476.
- M. Shrivastava, Q. Z. Rasool, B. Zhao, M. Octaviani, R. A. Zaveri, A. Zelenyuk, B.
 Gaudet, Y. Liu, J. E. Shilling, J. Schneider, C. Schulz, M. Zöger, S. T. Martin, J. Ye, A.
 Guenther, R. F. Souza, M. Wendisch and U. Pöschl, Tight Coupling of Surface and In Plant Biochemistry and Convection Governs Key Fine Particulate Components over the
 Amazon Rainforest, ACS Earth and Space Chemistry, 2022, 6, 380-390.
- R. A. Zaveri, R. C. Easter, J. E. Shilling and J. H. Seinfeld, Modeling kinetic partitioning of secondary organic aerosol and size distribution dynamics: representing effects of volatility, phase state, and particle-phase reaction, *Atmospheric Chemistry and Physics*, 2014, 14, 5153-5181.
 - 35. C. Le, N. Xu, Q. Li, D. R. Collins and D. R. Cocker, Experimental characterization of particle wall-loss behaviors in UCR dual-90m ³ Teflon chambers, *Aerosol Science and Technology*, 2024, **58**, 288-300.
 - 36. M. S. Taylor, Jr., D. N. Higgins, J. M. Krasnomowitz and M. V. Johnston, Ultrafine Particle Growth Rate During Biogenic Secondary Organic Matter Formation as a Function of Particle Composition, Size, and Phase, ACS ES&T Air, 2025, 2, 615-624.
 - M. Shiraiwa, C. Pfrang, T. Koop and U. Pöschl, Kinetic multi-layer model of gas-particle interactions in aerosols and clouds (KM-GAP): linking condensation, evaporation and chemical reactions of organics, oxidants and water, *Atmospheric Chemistry and Physics*, 2012, **12**, 2777-2794.
 - 38. J. H. Seinfeld and S. N. Pandis, *Atmospheric chemistry and physics : from air pollution to climate change*, John Wiley & Sons, Inc., Hoboken, New Jersey, Third edition edn., 2016.
 - 39. M. Z. Jacobson and R. P. Turco, Simulating Condensational Growth, Evaporation, and Coagulation of Aerosols Using a Combined Moving and Stationary Size Grid, *Aerosol Science and Technology*, 1995, **22**, 73-92.
- M. Z. Jacobson, D. B. Kittelson and W. F. Watts, Enhanced Coagulation Due to
 Evaporation and Its Effect on Nanoparticle Evolution, *Environmental Science & English Technology*, 2005, 39, 9486-9492.
- J. Julin, P. M. Winkler, N. M. Donahue, P. E. Wagner and I. Riipinen, Near-Unity Mass
 Accommodation Coefficient of Organic Molecules of Varying Structure, *Environmental Science & Science &*
- M. Von Domaros, P. S. J. Lakey, M. Shiraiwa and D. J. Tobias, Multiscale Modeling of
 Human Skin Oil-Induced Indoor Air Chemistry: Combining Kinetic Models and
 Molecular Dynamics, *The Journal of Physical Chemistry B*, 2020, 124, 3836-3843.
- 43. Y. Li and M. Shiraiwa, Timescales of secondary organic aerosols to reach equilibrium at various temperatures and relative humidities, *Atmospheric Chemistry and Physics*, 2019, **19**, 5959-5971.
- V.-M. Kerminen, K. E. J. Lehtinen, T. Anttila and M. Kulmala, Dynamics of atmospheric nucleation mode particles: a timescale analysis, *Tellus B*, 2004, **56**, 135-146.
- A. D'Alessio, A. C. Barone, R. Cau, A. D'Anna and P. Minutolo, Surface deposition and coagulation efficiency of combustion generated nanoparticles in the size range from 1 to 10 nm, *Proceedings of the Combustion Institute*, 2005, **30**, 2595-2603.
- G. Narsimhan and E. Ruckenstein, Monte Carlo simulation of brownian coagulation over the entire range of particle sizes from near molecular to colloidal: Connection between

626 627

634

635

636

637

638

639

640

641

642

643 644

645

646

647

648 649

650

- collision efficiency and interparticle forces, *Journal of Colloid and Interface Science*,
 1985, **107**, 174-193.
- D. Hou, D. Zong, C. S. Lindberg, M. Kraft and X. You, On the coagulation efficiency of carbonaceous nanoparticles, *Journal of Aerosol Science*, 2020, **140**, 105478.
- 48. A. Virtanen, J. Kannosto, H. Kuuluvainen, A. Arffman, J. Joutsensaari, E. Saukko, L.
 Hao, P. Yli-Pirilä, P. Tiitta, J. K. Holopainen, J. Keskinen, D. R. Worsnop, J. N. Smith
 and A. Laaksonen, Bounce behavior of freshly nucleated biogenic secondary organic
 aerosol particles, *Atmospheric Chemistry and Physics*, 2011, 11, 8759-8766.
 - 49. S. Mahant, J. R. Snider, S. S. Petters and M. D. Petters, Effect of Aerosol Size on Glass Transition Temperature, *The Journal of Physical Chemistry Letters*, 2024, **15**, 7509-7515.
- 628 50. M. Petters and S. Kasparoglu, Predicting the influence of particle size on the glass transition temperature and viscosity of secondary organic material, *Scientific Reports*, 2020, **10**.
- M. Kulmala, M. D. Maso, J. M. Makela, L. Pirjola, M. Vakeva, P. Aalto, P.
 Miikkulainen, K. Hameri and C. D. O'Dowd, On the formation, growth and composition of nucleation mode particles, *Tellus B*, 2001, 53, 479-490.
 - 52. M. Shiraiwa and U. Pöschl, Mass accommodation and gas—particle partitioning in secondary organic aerosols: dependence on diffusivity, volatility, particle-phase reactions, and penetration depth, *Atmospheric Chemistry and Physics*, 2021, **21**, 1565-1580.
 - C. Rose, M. Collaud Coen, E. Andrews, Y. Lin, I. Bossert, C. Lund Myhre, T. Tuch, A. 53. Wiedensohler, M. Fiebig, P. Aalto, A. Alastuey, E. Alonso-Blanco, M. Andrade, B. Artíñano, T. Arsov, U. Baltensperger, S. Bastian, O. Bath, J. P. Beukes, B. T. Brem, N. Bukowiecki, J. A. Casquero-Vera, S. Conil, K. Eleftheriadis, O. Favez, H. Flentje, M. I. Gini, F. J. Gómez-Moreno, M. Gysel-Beer, A. G. Hallar, I. Kalapov, N. Kalivitis, A. Kasper-Giebl, M. Keywood, J. E. Kim, S.-W. Kim, A. Kristensson, M. Kulmala, H. Lihavainen, N.-H. Lin, H. Lyamani, A. Marinoni, S. Martins Dos Santos, O. L. Mayol-Bracero, F. Meinhardt, M. Merkel, J.-M. Metzger, N. Mihalopoulos, J. Ondracek, M. Pandolfi, N. Pérez, T. Petäjä, J.-E. Petit, D. Picard, J.-M. Pichon, V. Pont, J.-P. Putaud, F. Reisen, K. Sellegri, S. Sharma, G. Schauer, P. Sheridan, J. P. Sherman, A. Schwerin, R. Sohmer, M. Sorribas, J. Sun, P. Tulet, V. Vakkari, P. G. Van Zyl, F. Velarde, P. Villani, S. Vratolis, Z. Wagner, S.-H. Wang, K. Weinhold, R. Weller, M. Yela, V. Zdimal and P. Lai, Seasonality of the particle number concentration and size distribution: a global analysis retrieved from the network of Global Atmosphere Watch (GAW) near-surface observatories, Atmospheric Chemistry and Physics, 2021, 21, 17185-17223.
- 54. S. Gani, S. Bhandari, K. Patel, S. Seraj, P. Soni, Z. Arub, G. Habib, L. Hildebrandt Ruiz and J. S. Apte, Particle number concentrations and size distribution in a polluted megacity: the Delhi Aerosol Supersite study, *Atmospheric Chemistry and Physics*, 2020, 20, 8533-8549.
- 657 55. M. Shiraiwa and J. H. Seinfeld, Equilibration timescale of atmospheric secondary organic aerosol partitioning, *Geophysical Research Letters*, 2012, **39**, n/a-n/a.
- I. Riipinen, J. R. Pierce, T. Yli-Juuti, T. Nieminen, S. Häkkinen, M. Ehn, H. Junninen, K.
 Lehtipalo, T. Petäjä, J. Slowik, R. Chang, N. C. Shantz, J. Abbatt, W. R. Leaitch, V. M.
 Kerminen, D. R. Worsnop, S. N. Pandis, N. M. Donahue and M. Kulmala, Organic

681

682

683

684

685

686

687

688

689

690

691

692 693

694

695

696

697

- condensation: a vital link connecting aerosol formation to cloud condensation nuclei (CCN) concentrations, *Atmospheric Chemistry and Physics*, 2011, **11**, 3865-3878.
- H. Mai, M. Shiraiwa, R. C. Flagan and J. H. Seinfeld, Under What Conditions Can
 Equilibrium Gas-Particle Partitioning Be Expected to Hold in the Atmosphere?,
 Environmental Science & Environmental Science & Technology, 2015, 49, 11485-11491.
- R. J. Griffin, D. R. Cocker, R. C. Flagan and J. H. Seinfeld, Organic aerosol formation from the oxidation of biogenic hydrocarbons, *Journal of Geophysical Research:* Atmospheres, 1999, 104, 3555-3567.
- R. K. Pathak, C. O. Stanier, N. M. Donahue and S. N. Pandis, Ozonolysis of α pinene
 at atmospherically relevant concentrations: Temperature dependence of aerosol mass
 fractions (yields), *Journal of Geophysical Research: Atmospheres*, 2007, 112.
- 673 60. C.-W. Chu, J. Zhai, Y. Han, J. Ye, R. A. Zaveri, S. T. Martin and H.-M. Hung, New
 674 Particle Formation and Growth Dynamics for α-Pinene Ozonolysis in a Smog Chamber
 675 and Implications for Ambient Environments, ACS Earth and Space Chemistry, 2022, 6,
 676 2826-2835.
- 61. V. G. Khamaganov and R. A. Hites, Rate Constants for the Gas-Phase Reactions of
 678 Ozone with Isoprene, α- and β-Pinene, and Limonene as a Function of Temperature, *The Journal of Physical Chemistry A*, 2001, **105**, 815-822.
 - 62. X. Zhang, S. N. Pandis and J. H. Seinfeld, Diffusion-Limited Versus Quasi-Equilibrium Aerosol Growth, *Aerosol Science and Technology*, 2012, **46**, 874-885.
 - 63. J. F. Hunter, A. J. Carrasquillo, K. E. Daumit and J. H. Kroll, Secondary Organic Aerosol Formation from Acyclic, Monocyclic, and Polycyclic Alkanes, *Environmental Science & Environmental Science*
 - 64. C. Kuang, I. Riipinen, S. L. Sihto, M. Kulmala, A. V. McCormick and P. H. McMurry, An improved criterion for new particle formation in diverse atmospheric environments, *Atmospheric Chemistry and Physics*, 2010, **10**, 8469-8480.
 - 65. J. Kirkby, J. Curtius, J. Almeida, E. Dunne, J. Duplissy, S. Ehrhart, A. Franchin, S. Gagné, L. Ickes, A. Kürten, A. Kupc, A. Metzger, F. Riccobono, L. Rondo, S. Schobesberger, G. Tsagkogeorgas, D. Wimmer, A. Amorim, F. Bianchi, M. Breitenlechner, A. David, J. Dommen, A. Downard, M. Ehn, R. C. Flagan, S. Haider, A. Hansel, D. Hauser, W. Jud, H. Junninen, F. Kreissl, A. Kvashin, A. Laaksonen, K. Lehtipalo, J. Lima, E. R. Lovejoy, V. Makhmutov, S. Mathot, J. Mikkilä, P. Minginette, S. Mogo, T. Nieminen, A. Onnela, P. Pereira, T. Petäjä, R. Schnitzhofer, J. H. Seinfeld, M. Sipilä, Y. Stozhkov, F. Stratmann, A. Tomé, J. Vanhanen, Y. Viisanen, A. Vrtala, P. E. Wagner, H. Walther, E. Weingartner, H. Wex, P. M. Winkler, K. S. Carslaw, D. R. Worsnop, U. Baltensperger and M. Kulmala, Role of sulphuric acid, ammonia and galactic cosmic rays in atmospheric aerosol nucleation, *Nature*, 2011, 476, 429-433.
- W. Kong, S. Amanatidis, H. Mai, C. Kim, B. C. Schulze, Y. Huang, G. S. Lewis, S. V.
 Hering, J. H. Seinfeld and R. C. Flagan, The nano-scanning electrical mobility
 spectrometer (nSEMS) and its application to size distribution measurements of 1.5–25 nm
 particles, Atmospheric Measurement Techniques, 2021, 14, 5429-5445.
- D. Stolzenburg, L. Fischer, A. L. Vogel, M. Heinritzi, M. Schervish, M. Simon, A. C.
 Wagner, L. Dada, L. R. Ahonen, A. Amorim, A. Baccarini, P. S. Bauer, B. Baumgartner,
 A. Bergen, F. Bianchi, M. Breitenlechner, S. Brilke, S. Buenrostro Mazon, D. Chen, A.
 Dias, D. C. Draper, J. Duplissy, I. El Haddad, H. Finkenzeller, C. Frege, C. Fuchs, O.
 Garmash, H. Gordon, X. He, J. Helm, V. Hofbauer, C. R. Hoyle, C. Kim, J. Kirkby, J.

717

718

719

720

721

722

723

724

725

726

727

728

729

730

731

732

733

734

735

736

737

- 708 Kontkanen, A. Kürten, J. Lampilahti, M. Lawler, K. Lehtipalo, M. Leiminger, H. Mai, S. 709 Mathot, B. Mentler, U. Molteni, W. Nie, T. Nieminen, J. B. Nowak, A. Ojdanic, A. Onnela, M. Passananti, T. Petäjä, L. L. J. Quéléver, M. P. Rissanen, N. Sarnela, S. 710 711 Schallhart, C. Tauber, A. Tomé, R. Wagner, M. Wang, L. Weitz, D. Wimmer, M. Xiao, C. Yan, P. Ye, Q. Zha, U. Baltensperger, J. Curtius, J. Dommen, R. C. Flagan, M. 712 713 Kulmala, J. N. Smith, D. R. Worsnop, A. Hansel, N. M. Donahue and P. M. Winkler, 714 Rapid growth of organic aerosol nanoparticles over a wide tropospheric temperature 715 range, Proceedings of the National Academy of Sciences, 2018, 115, 9122-9127.
 - 68. F. Bianchi, T. Kurtén, M. Riva, C. Mohr, M. P. Rissanen, P. Roldin, T. Berndt, J. D. Crounse, P. O. Wennberg, T. F. Mentel, J. Wildt, H. Junninen, T. Jokinen, M. Kulmala, D. R. Worsnop, J. A. Thornton, N. Donahue, H. G. Kjaergaard and M. Ehn, Highly Oxygenated Organic Molecules (HOM) from Gas-Phase Autoxidation Involving Peroxy Radicals: A Key Contributor to Atmospheric Aerosol, *Chemical Reviews*, 2019, 119, 3472-3509.
 - 69. J. Zhao, J. Ortega, M. Chen, P. H. McMurry and J. N. Smith, Dependence of particle nucleation and growth on high-molecular-weight gas-phase products during ozonolysis of α-pinene, *Atmospheric Chemistry and Physics*, 2013, **13**, 7631-7644.
 - M. Wang, W. Kong, R. Marten, X.-C. He, D. Chen, J. Pfeifer, A. Heitto, J. Kontkanen, L. Dada, A. Kürten, T. Yli-Juuti, H. E. Manninen, S. Amanatidis, A. Amorim, R. Baalbaki, A. Baccarini, D. M. Bell, B. Bertozzi, S. Bräkling, S. Brilke, L. C. Murillo, R. Chiu, B. Chu, L.-P. De Menezes, J. Duplissy, H. Finkenzeller, L. G. Carracedo, M. Granzin, R. Guida, A. Hansel, V. Hofbauer, J. Krechmer, K. Lehtipalo, H. Lamkaddam, M. Lampimäki, C. P. Lee, V. Makhmutov, G. Marie, S. Mathot, R. L. Mauldin, B. Mentler, T. Müller, A. Onnela, E. Partoll, T. Petäjä, M. Philippov, V. Pospisilova, A. Ranjithkumar, M. Rissanen, B. Rörup, W. Scholz, J. Shen, M. Simon, M. Sipilä, G. Steiner, D. Stolzenburg, Y. J. Tham, A. Tomé, A. C. Wagner, D. S. Wang, Y. Wang, S. K. Weber, P. M. Winkler, P. J. Wlasits, Y. Wu, M. Xiao, Q. Ye, M. Zauner-Wieczorek, X. Zhou, R. Volkamer, I. Riipinen, J. Dommen, J. Curtius, U. Baltensperger, M. Kulmala, D. R. Worsnop, J. Kirkby, J. H. Seinfeld, I. El-Haddad, R. C. Flagan and N. M. Donahue, Rapid growth of new atmospheric particles by nitric acid and ammonia condensation, *Nature*, 2020, 581, 184-189.
- 739 71. Y. Cheng, H. Su, T. Koop, E. Mikhailov and U. Pöschl, Size dependence of phase transitions in aerosol nanoparticles, *Nature Communications*, 2015, **6**.
- 741 72. K. M. Sakamoto, J. D. Allan, H. Coe, J. W. Taylor, T. J. Duck and J. R. Pierce, Aged
 742 boreal biomass-burning aerosol size distributions from BORTAS 2011, *Atmospheric Chemistry and Physics*, 2015, 15, 1633-1646.
- 74. K. M. Sakamoto, J. R. Laing, R. G. Stevens, D. A. Jaffe and J. R. Pierce, The evolution of biomass-burning aerosol size distributions due to coagulation: dependence on fire and meteorological details and parameterization, *Atmospheric Chemistry and Physics*, 2016, 747
 16, 7709-7724.
- 748 74. E. J. T. Levin, G. R. McMeeking, C. M. Carrico, L. E. Mack, S. M. Kreidenweis, C. E. Wold, H. Moosmüller, W. P. Arnott, W. M. Hao, J. L. Collett and W. C. Malm, Biomass burning smoke aerosol properties measured during Fire Laboratory at Missoula Experiments (FLAME), *Journal of Geophysical Research: Atmospheres*, 2010, **115**.
- 752 75. N. A. June, A. L. Hodshire, E. B. Wiggins, E. L. Winstead, C. E. Robinson, K. L. Thornhill, K. J. Sanchez, R. H. Moore, D. Pagonis, H. Guo, P. Campuzano-Jost, J. L.

767

768

769

770

771

772

773

774

775

- Jimenez, M. M. Coggon, J. M. Dean-Day, T. P. Bui, J. Peischl, R. J. Yokelson, M. J. Alvarado, S. M. Kreidenweis, S. H. Jathar and J. R. Pierce, Aerosol size distribution changes in FIREX-AQ biomass burning plumes: the impact of plume concentration on coagulation and OA condensation/evaporation, *Atmospheric Chemistry and Physics*, 2022, 22, 12803-12825.
- 76. L. A. Garofalo, M. A. Pothier, E. J. T. Levin, T. Campos, S. M. Kreidenweis and D. K.
 760 Farmer, Emission and Evolution of Submicron Organic Aerosol in Smoke from Wildfires
 761 in the Western United States, ACS Earth and Space Chemistry, 2019, 3, 1237-1247.
- 762 77. A. A. May, E. J. T. Levin, C. J. Hennigan, I. Riipinen, T. Lee, J. L. Collett, J. L. Jimenez,
 763 S. M. Kreidenweis and A. L. Robinson, Gas particle partitioning of primary organic
 764 aerosol emissions: 3. Biomass burning, *Journal of Geophysical Research: Atmospheres*,
 765 2013, 118, 11,327-311,338.
 - 78. J. A. Huffman, K. S. Docherty, A. C. Aiken, M. J. Cubison, I. M. Ulbrich, P. F. Decarlo, D. Sueper, J. T. Jayne, D. R. Worsnop, P. J. Ziemann and J. L. Jimenez, Chemically-resolved aerosol volatility measurements from two megacity field studies, *Atmospheric Chemistry and Physics*, 2009, **9**, 7161-7182.
 - 79. Y. Huang, F. Mahrt, S. Xu, M. Shiraiwa, A. Zuend and A. K. Bertram, Coexistence of three liquid phases in individual atmospheric aerosol particles, *Proceedings of the National Academy of Sciences*, 2021, **118**, e2102512118.
 - 80. N. G. A. Gerrebos, J. Zaks, F. K. A. Gregson, M. Walton-Raaby, H. Meeres, I. Zigg, W. F. Zandberg and A. K. Bertram, High Viscosity and Two Phases Observed over a Range of Relative Humidities in Biomass Burning Organic Aerosol from Canadian Wildfires, *Environmental Science & Environmental Science* & 2024, 58, 21716-21728.
- A. L. Hodshire, Q. Bian, E. Ramnarine, C. R. Lonsdale, M. J. Alvarado, S. M.
 Kreidenweis, S. H. Jathar and J. R. Pierce, More Than Emissions and Chemistry: Fire
 Size, Dilution, and Background Aerosol Also Greatly Influence Near Field Biomass
 Burning Aerosol Aging, *Journal of Geophysical Research: Atmospheres*, 2019, 124,
 5589-5611.
- 782 82. P. S. Lee and D. T. Shaw, Dynamics of Fibrous-Type Particles: Brownian Coagulation and the Charge Effect, *Aerosol Science and Technology*, 1984, **3**, 9-16.
- V. I. Gryn and M. K. Kerimov, Integrodifferential equations for non-spherical aerosols coagulation, *USSR Computational Mathematics and Mathematical Physics*, 1990, 30, 211-224.
- 787 84. S. N. Rogak and R. C. Flagan, Coagulation of aerosol agglomerates in the transition regime, *Journal of Colloid and Interface Science*, 1992, **151**, 203-224.
- 789 85. T. Hawa and M. R. Zachariah, Coalescence kinetics of unequal sized nanoparticles, 790 *Journal of Aerosol Science*, 2006, **37**, 1-15.
- 791 86. L. A. Spielman, Viscous interactions in Brownian coagulation, *Journal of Colloid and Interface Science*, 1970, **33**, 562-571.
- 793 K. Higashitani, M. Kondo and S. Hatade, Effect of particle size on coagulation rate of ultrafine colloidal particles, *Journal of Colloid and Interface Science*, 1991, **142**, 204-213.
- R. M. Power, S. H. Simpson, J. P. Reid and A. J. Hudson, The transition from liquid to solid-like behaviour in ultrahigh viscosity aerosol particles, *Chemical Science*, 2013, **4**, 2597.

800

801

802

803

89. D. M. Bell, D. Imre, S. T. Martin and A. Zelenyuk, The properties and behavior of α-pinene secondary organic aerosol particles exposed to ammonia under dry conditions, *Physical Chemistry Chemical Physics*, 2017, **19**, 6497-6507.

This article is licensed under a Creative Commons Attribution 3.0 Unported Licence.

Open Access Article. Published on 14 nuvembre 2025. Downloaded on 19/11/2025 1:24:40.

The simulation data may be obtained from the corresponding author upon request.